The EMBO Journal (2013) 32, 496–510
www.embojournal.org

SOURCE DATA | TRANSPARENT PROCESS

THE EMBO JOURNAL

CaMKII-dependent phosphorylation of GluK5 mediates plasticity of kainate receptors

Mario Carta[1,2], Patrizio Opazo[1,2], Julien Veran[1,2], Axel Athané[1,2], Daniel Choquet[1,2], Françoise Coussen[1,2,3] and Christophe Mulle[1,2,3,*]

[1]Université Bordeaux, Institut Interdisciplinaire de Neurosciences, UMR 5297, Bordeaux, France and [2]CNRS, Institut Interdisciplinaire de Neurosciences, UMR 5297, Bordeaux, France

Calmodulin-dependent kinase II (CaMKII) is key for long-term potentiation of synaptic AMPA receptors. Whether CaMKII is involved in activity-dependent plasticity of other ionotropic glutamate receptors is unknown. We show that repeated pairing of pre- and postsynaptic stimulation at hippocampal mossy fibre synapses induces long-term depression of kainate receptor (KAR)-mediated responses, which depends on Ca^{2+} influx, activation of CaMKII, and on the GluK5 subunit of KARs. CaMKII phosphorylation of three residues in the C-terminal domain of GluK5 subunit markedly increases lateral mobility of KARs, possibly by decreasing the binding of GluK5 to PSD-95. CaMKII activation also promotes surface expression of KARs at extrasynaptic sites, but concomitantly decreases its synaptic content. Using a molecular replacement strategy, we demonstrate that the direct phosphorylation of GluK5 by CaMKII is necessary for KAR-LTD. We propose that CaMKII-dependent phosphorylation of GluK5 is responsible for synaptic depression by untrapping of KARs from the PSD and increased diffusion away from synaptic sites.

The EMBO Journal (2013) **32,** 496–510. doi:10.1038/emboj.2012.334; Published online 4 January 2013
Subject Categories: neuroscience
Keywords: CaMKII; glutamate receptors; hippocampal mossy fibres; kainate receptors; plasticity

Introduction

Ca^{2+}/calmodulin-dependent kinase II (CaMKII), a major constituent of excitatory synapses is central to the regulation of glutamatergic synapses (Lisman *et al*, 2002) and to the induction of long-term potentiation (LTP). The recruitment and activation of CaMKII following activation of NMDA receptors leads to an increase in the number of synaptic AMPA receptors (AMPAR) (Lisman *et al*, 2002; Opazo and Choquet, 2011). CaMKII regulates the function and trafficking of AMPARs at synapses, through mechanisms that involve the phosphorylation of either AMPARs, or AMPAR interacting proteins. CaMKII phosphorylation of the AMPAR subunit GluA1 (on serine 831), leads to enhancement of AMPAR channel function (Barria *et al*, 1997; Mammen *et al*, 1997; Kristensen *et al*, 2011). Activity-dependent recruitment of AMPARs at synapses also involves an immobilization mechanism (Makino and Malinow, 2009) as a result of the CaMKII-dependent phosphorylation of stargazin (Opazo *et al*, 2010).

The role of CaMKII in controlling the trafficking or function of kainate receptors (KARs), a family of ionotropic glutamate receptors involved in the regulation and plasticity of synaptic networks (Contractor *et al*, 2011) is currently unknown. KARs share many structural and biophysical similarities with AMPARs, but also display marked functional specificities that could have profound consequences on their ability to shape synaptic transmission (Perrais *et al*, 2010). At hippocampal mossy fibre–CA3 pyramidal cell synapses (mf-CA3 synapses), KARs likely composed of GluK2, GluK4 and GluK5 subunits (Mulle *et al*, 1998; Contractor *et al*, 2003; Fernandes *et al*, 2009) mediate postsynaptic inward currents (KAR-EPSCs) involved in the integration of synaptic signals (Pinheiro *et al*, 2012).

Several studies indicate that PKC activation regulate KAR trafficking to the membrane (Hirbec *et al*, 2003; Martin and Henley, 2004; Rivera *et al*, 2007) and is involved in activity-dependent synaptic depression of KARs (Park *et al*, 2006; Selak *et al*, 2009). Because major forms of synaptic plasticity depend on the Ca^{2+}-dependent activation of CaMKII, we have studied the possible role of CaMKII-dependent in the regulation of trafficking and function of KARs, and its involvement in the plasticity of synaptic KARs. A spike-timing-dependent protocol that induces potentiation of AMPA-EPSCs at conventional excitatory synapses via a CaMKII-dependent mechanism, leads to long-term depression of KAR-EPSCs (KAR-LTD) at mf-CA3 synapses. We show that KAR-LTP operated through a novel synaptic untrapping mechanism, which directly depends on the phosphorylation of the GluK5 KAR subunit.

Results

Repeated pairing of pre- and postsynaptic stimulation leads to LTD of KARs

We tested the possibility that CaMKII is involved in the activity-dependent plasticity of KAR-EPSPs at mf-CA3 synapses using a spike-timing-dependent plasticity (STDP) protocol known to trigger activation of CaMKII and induction of LTP at other synapses (Caporale and Dan, 2008) (Figure 1). In mouse organotypic hippocampal slices, a protocol consisting of the positive pairing of presynaptic stimulations to postsynaptic backpropagating action potentials (see Materials and methods) (Figure 1A) induced a long-lasting decrease in the amplitude of pharmacologically isolated

*Corresponding author. Institute for Interdisciplinary Neuroscience, University of Bordeaux, CNRS UMR 5297, CNRS, 146 Avenue Léo Saignat, Bordeaux 33000, France. Tel.: +33 6 26 01 61 74; Fax: +33 5 57 57 40 82; E-mail: mulle@u-bordeaux2.fr
[3]These two authors are equal senior authors

Received: 22 August 2012; accepted: 16 November 2012; published online: 4 January 2013

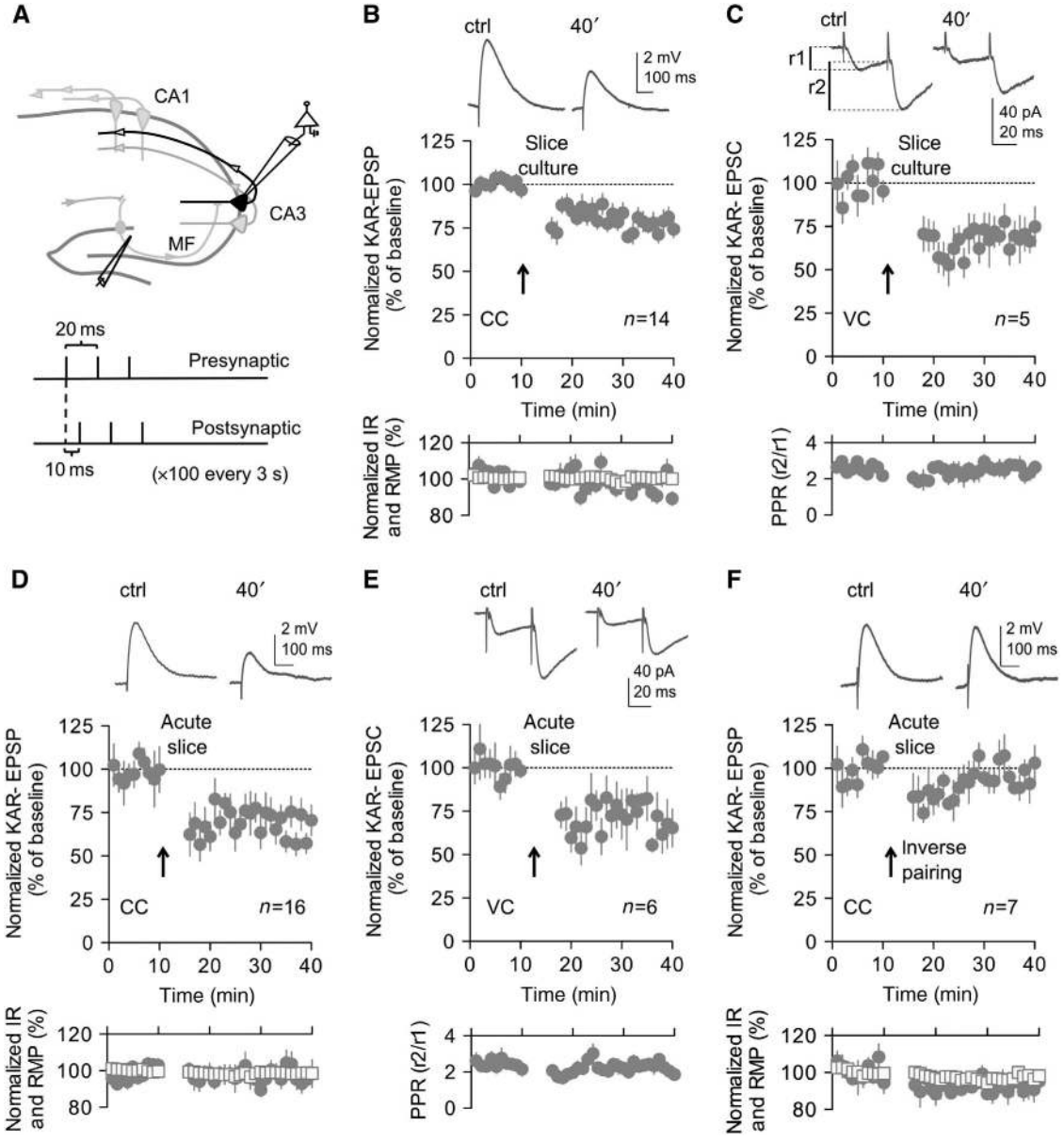

Figure 1 Repeated pairing of pre- and postsynaptic stimulation leads to KAR-LTD in slice cultures and acute slices. (**A**) Illustrative scheme of the hippocampus with recording and stimulating electrodes. Lower part, stimulating protocol used to induce KAR-LTD. (**B**) In slice cultures prepared from WT mice, in current clamp (CC) the STDP-like pairing protocol induces LTD of pharmacologically isolated (50 μM GYKI53655) KAR-EPSPs (74.4 ± 5.0%, $n = 14$, of baseline values 30–40 min after induction). (**B–F**) In the inserts are shown representative sample traces of KAR-EPSPs (or KAR-EPSCs) (10 averaged traces) before and after the induction protocol. (**B**, **D**, **F**) Input resistance (empty squares) and resting membrane potential (filled circles) remained stable throughout the experiment. (**C**) Time course of KAR-LTD recorded in voltage clamp (VC) (78.1 ± 5.3%, $n = 5$). No change in PPR (lower panels), indicating an absence of a presynaptic locus of expression for KAR-LTD (PPR of 2.6 ± 0.8 and 2.6 ± 0.3, respectively, during baseline and after LTD; $n = 5$). (**D–F**) Experiments in acute slices prepared from WT mice (P17–19). (**D**) In the current-clamp mode, the STDP-like protocol induces LTD of KAR-EPSPs to a similar extent as in organotypic slice culture (65.6 ± 4.0%, $n = 16$, $P < 0.001$). (**E**) KAR-LTD is also observed in the voltage-clamp mode (77.1 ± 7.7%, $n = 6$, $P < 0.01$) and is not accompanied with changes in the paired-pulse ratio (PPR of 2.4 ± 0.2 and 2.3 ± 0.2, respectively, during baseline and after LTD; $n = 6$). (**F**) Inverting the timing of the pre- and postsynaptic stimulation (the postsynaptic triplets preceding by 10 ms the presynaptic stimulation) did not lead to long-lasting changes in KAR-EPSPs (95.2 ± 2.5%, $n = 7$). Values are presented as mean ± s.e.m. of n experiments.

(50 μM GYKI53655; Supplementary Figure S1C) KAR-EPSPs at mf-CA3 synapses (KAR-LTD) ($P < 0.001$) (Figures 1B and 2G). The amplitude of KAR-EPSPs did not change over 40 min in the absence of the induction protocol (Supplementary Figure S2C and F). Moreover, no change in the amplitude of KAR-EPSPs was observed if only postsynaptic spike triggering or presynaptic stimulation were applied independently (Supplementary Figure S2D–F). No long-lasting change in the paired-pulse ratio (Figure 1C), or coefficient of variation (Supplementary Figure S2G) was observed when monitoring KAR-EPSCs, indicating a postsynaptic locus of expression of KAR-LTD. This was confirmed by the lack of effect of the STDP-like protocol on AMPAR-EPSPs (Supplementary Figure S2F). KAR-LTD could also be induced in acute wild-type (WT) mouse slices in both the current-clamp ($P < 0.001$) (Figure 1D) and the voltage-clamp modes ($P < 0.01$)

(Figure 1E). Inverting the timing of the pre- and postsynaptic stimulation did not lead to long-lasting changes in KAR-EPSPs (Figure 1F), suggesting that precise timing is needed for the induction of this new form of plasticity.

KAR-LTD: dependency on CaMKII and GluK5

Subsequent results were obtained from slice cultures, because this allows molecular rescue experiments. KAR-LTD was prevented when the slices were bathed with the L-VGCC blockers nifedipine (Figure 2A and H) or nimodipine (Supplementary Figure S3C). KAR-LTD was also abolished by inclusion of BAPTA in the intracellular solution (Figure 2H), clearly indicating that KAR-LTD depends on a rise in postsynaptic Ca^{2+} via opening of L-VGCC. A general mGluR antagonist LY341495 (Figure 2B and H), or a cocktail containing mGluR1 and mGluR5 antagonists (MPEP and CPCC) (Supplementary Figure S3C) did not inhibit KAR-LTD ($P<0.001$ and $P<0.01$, respectively). Preincubation of the slice with the NMDAR antagonists D-AP5 or MK801 (Figure 2H; Supplementary Figure S3A and C), failed to block KAR-LTD ($P<0.001$ and <0.01, respectively). These results indicate an involvement of L-VGCC but not of NMDARs, AMPARs or mGluRs in KAR-LTD. Because presynaptic activity (paired with postsynaptic activity) is required for KAR-LTD, we tested whether synaptically released glutamate acting on KARs themselves was involved in LTD. For this, kynurenate, a broad spectrum iGluR antagonist, was applied before and during the LTD induction protocol, and washed out 10 min after. KAR-EPSPs recovered to baseline levels after 45 min (Figure 2C and H). These experiments indicate that synaptic KARs are involved in KAR-LTD. Notably, washing the slice of kynurenate without delivering the stimulation protocol did not cause any significant effect to the synaptic response (Figure 2H; Supplementary Figure S3B).

Finally, downstream of Ca^{2+} rise, KAR-LTD required the activation of CaMKII, since no depression was observed after the application of the STDP stimulation protocol in the presence of the CaMKII inhibitor KN93 in the bath (Figure 2H). In order to confirm this pharmacological result, we biolistically transfected CA3 pyramidal cell with K42R, a CaMKII mutant that lacks kinase activity, and acts as a dominant negative mutant for CaMKII (Shen and Meyer, 1999; Yamagata *et al*, 2009). We found that KAR-LTD was completely abrogated 24–36 h after transfection ((Figure 2D and H) (Supplementary Figure S3D).

Two studies have recently shown that synaptic depression of KAR responses at mf-CA3 synapses could involve PKC activity (Selak *et al*, 2009; Chamberlain *et al*, 2012). Interestingly, we found that perfusion with two different PKC inhibitors, Ro318220 and chelerythrine, also abrogated KAR-LTD induced by the STDP protocol (Figure 2E and H) (Supplementary Figure S3C). PKC phosphorylation of KARs has been shown to promote endocytosis (Selak *et al*, 2009; Chamberlain *et al*, 2012). We have tested if endocytosis of KARs was determinant for KAR-LTD induced by the STDP like protocol. Interestingly, we found that KAR-LTD was not affected by the inclusion in the patch pipette of the D15 peptide ($P<0.01$) (Figure 2F and H) (Luscher *et al*, 1999), or dynasore, which blocks endocytosis by rapid inhibition the GTPase activity of dynamin ($P<0.01$) (Supplementary Figure S3C and E) (Newton *et al*, 2006; Jaskolski *et al*, 2009).

Finally, a previously described form of LTD of KAR-EPSCs requires GluK5 (Selak *et al*, 2009), a major component of postsynaptic KARs at mf-CA3 synapses (Contractor *et al*, 2003; Ruiz *et al*, 2005). We observed that KAR-LTD induced by the STDP-like protocol, was also absent in GluK5$^{-/-}$ mice both in slice cultures and in acute slices (Figure 2G and H) (Supplementary Figure S3F), indicating a crucial role for this subunit in the plasticity of KARs. Hence, although KAR-LTD induced by the STDP protocol requires activation of PKC, its mechanism is clearly different from the previously reported forms of KAR-LTD (Selak *et al*, 2009; Chamberlain *et al*, 2012). Indeed, in contrast with these forms of synaptic depression, STDP-like protocol induces LTD of KARs by mechanisms which involve activation of KARs, Ca^{2+} influx through L-VGCC and activation of CaMKII, and which do not seem to rely primarily on endocytosis.

GluK5 is phosphorylated by CaMKII in vitro

We investigated whether GluK5 is itself a substrate of CaMKII-dependent phosphorylation using *in vitro* phosphorylation assay (Figure 3). GluK5 C-terminal domain comprises 155 amino acids containing three potential CaMKII phosphorylation sites (R/K-X-X-S/T-X) at S^{859}, S^{892} and T^{976} (Figure 3A). We generated GST-fusion proteins with the intracellular C-terminal domain of GluK5 and performed *in vitro* phosphorylation with (γ^{32}P)-ATP and purified CaMKII. The phosphorylated proteins were subjected to SDS–PAGE, blot transfer and immunolabelling of GluK5 (Figure 3B). The C-terminal domain of GluK5 can be phosphorylated *in vitro* by CaMKII (Figure 3B). Mutants of the GluK5 C-terminal domain were then generated, in which only one of the consensus CaMKII sites could be phosphorylated, the other two sites being mutated into alanine. Each of these three sites can be phosphorylated by CaMKII *in vitro* albeit to a lesser extent than that for the WT proteins. As a control, a GST-GluK5 mutant in which the three consensus sites are mutated into alanine (GluK5AAA) cannot be phosphorylated,

Figure 2 Mechanisms of KAR-LTD: dependency on CaMKII and GluK5. All electrophysiological experiments presented in this figure are performed in the current-clamp mode. (**A**) Bath perfusion of nifedipine (20 μM) abrogated KAR-LTD (94.1 ± 3.7%, $n=6$). (**A–F**) In the inserts are shown representative sample traces of KAR-EPSPs (10 averaged traces) before and after the induction protocol. (**A–F**) Input resistance (empty squares) and resting membrane potential (filled circles) remained stable throughout the experiment. (**B**) LTD of KAR-EPSPs was not abrogated by bath perfusion of LY341495 (100 μM) (77.8 ± 5.6%, $n=6$ $P<0.001$). (**C**) Perfusion of kynurenate (3 mM) before and during the induction protocol abrogated KAR-LTD (96.4 ± 8.1%, $n=8$). In the insert are shown representative sample traces of KAR-EPSPs before, during and after the perfusion of kynurenate. (**D**) CA3 pyramidal cells transfected with CaMKII-K42R did not display KAR-LTD (94.5 ± 6.8%, $n=9$). (**E**) Perfusion with two different PKC inhibitors, Ro318220 (3 μM), also abrogated KAR-LTD (96.9 ± 6.1%, $n=5$). (**F**) KAR-LTD was not affected by postsynaptic infusion of D15 (1.5 mM) (74.1 ± 7.3%, $n=8$, $P<0.01$). (**G**) In slices prepared from GluK5$^{-/-}$ mice, the STDP-like protocol failed to induce LTD of KAR-EPSPs (104.1 ± 7.5%, $n=13$). (**H**) Summary of changes of KAR-EPSP amplitudes after the STDP-like protocol, in different experimental conditions as indicated (BAPTA (20 mM): 102.4 ± 7.4%, $n=6$) (KN93 (10 μM): 93.9 ± 5.2%, $n=8$). Values are presented as mean ± s.e.m. of n experiments. Data were compared using unpaired t-test (**$P<0.01$).

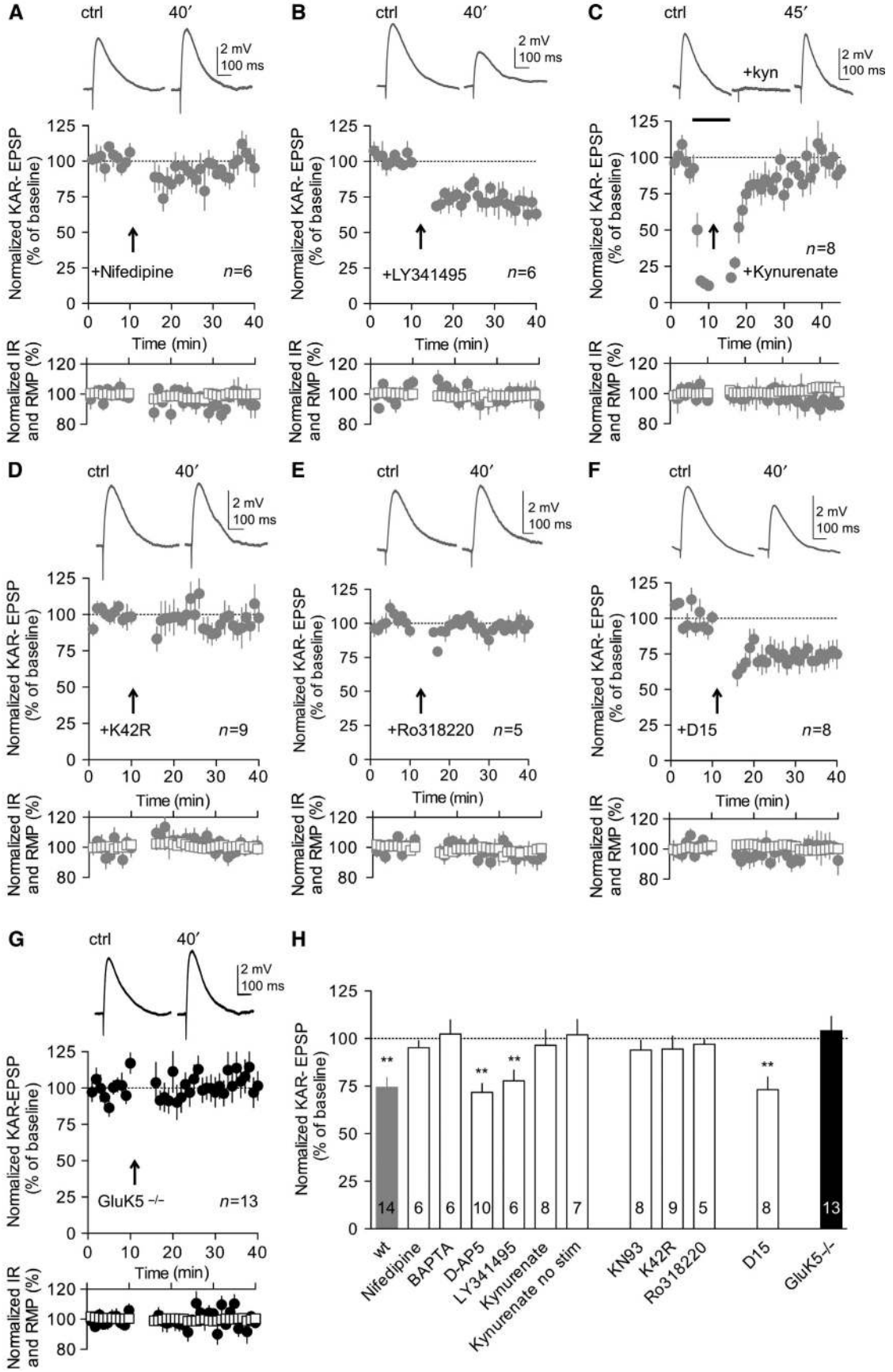
A
ctrl
40′
2 mV
100 ms
Normalized KAR- EPSP (% of baseline)
+Nifedipine
n=6
Time (min)
Normalized IR and RMP (%)
B
ctrl
40′
2 mV
100 ms
+LY341495
n=6
C
ctrl
45′
+kyn
2 mV
100 ms
n=8
+Kynurenate
D
ctrl
40′
2 mV
100 ms
+K42R
n=9
E
ctrl
40′
2 mV
100 ms
+Ro318220
n=5
F
ctrl
40′
2 mV
100 ms
+D15
n=8
G
ctrl
40′
2 mV
100 ms
Normalized KAR-EPSP (% of baseline)
GluK5 -/-
n=13
H
Normalized KAR- EPSP (% of baseline)
14
6
6
10
6
8
7
8
9
5
8
13
wt
Nifedipine
BAPTA
D-AP5
LY341495
Kynurenate
Kynurenate no stim
KN93
K42R
Ro318220
D15
GluK5-/-

indicating the absence of other CaMKII phosphorylation sites in the C-terminal domain of GluK5.

Properties of GluK5 phosphorylation mutants

We characterized the impact of mutating CaMKII phosphorylation sites on the trafficking and functional properties of GluK5 in heterologous expression systems. GluK5 strongly controls the expression of heteromeric GluK2/GluK5 KARs at the plasma membrane due to endoplasmic reticulum (ER) retention motifs in its C-terminal domain (Gallyas *et al*, 2003; Ren *et al*, 2003; Nasu-Nishimura *et al*, 2006). We thus examined plasma membrane expression of the myc-tagged GluK5 mutants assembled with either one of the GluK2 splice variants GluK2a or GluK2b in COS-7 cells (Figure 3C). Co-transfection of GluK2a with GluK5 increased surface expression of GluK5wt as previously shown (Nasu-Nishimura *et al*, 2006). No significant difference in the relative amount of GluK5 (or GluK2a) exported to the plasma membrane was observed when the phospho-null (GluK5AAA) or the phospho-mimetic (GluK5DDD) mutants of GluK5 were expressed with GluK2a (Figure 3C). When assembled with GluK2b, surface expression of GluK5wt and GluK5AAA was slightly lower than with GluK2a (Figure 3C). In contrast, the phospho-mimetic mutant GluK5DDD slightly enhanced surface expression of the GluK2b/GluK5 heteromer (both surface GluK2b and GluK5DDD increase) ($P<0.05$) (Figure 3C). These experiments are in general consistent with the electrophysiological analysis of recombinant GluK2/GluK5 receptors expressed in HEK 293 cells (Supplementary Figure S4).

Phosphorylation of GluK5 increases surface expression and decreases synaptic content of KARs in cultured hippocampal neurons

The impact of GluK5 mutations on the surface expression of myc–GluK5wt was analysed in cultured hippocampal neurons derived from GluK2$^{-/-}$ x GluK5$^{-/-}$ mice (Figure 4A and B). Following co-transfection of myc–GluK5 with either GluK2a or GluK2b, extracellular and total expression of GluK5 were detected with anti-myc antibodies (Figure 4A). Myc–GluK5wt and myc–GluK5AAA co-expressed with GluK2a or GluK2b were present at the plasma membrane in comparable amounts (Figure 4B) to that reported in WT hippocampal neurons (Nasu-Nishimura *et al*, 2006). Expression of myc–GluK5DDD with either GluK2a or GluK2b subunits markedly increased surface expression of GluK2/GluK5 receptors ($P<0.001$).

To confirm the role of CaMKII-dependent phosphorylation of GluK5wt, neurons from KO mice were co-transfected with GluK2a/myc–GluK5wt or GluK2b/myc–GluK5wt and either wt CaMKII or a truncated constitutively active CaMKII (tCaMKII). TCaMKII markedly increased surface expression of GluK5 when co-assembled with either GluK2a or GluK2b ($P<0.001$) (Figure 4C). As a control, expression of tCaMKII did not change the plasma membrane localization of GluK5AAA, which cannot be phosphorylated, when expressed with either GluK2a or GluK2b (Figure 4C). Interestingly, the levels reached for the amount of surface expressed GluK5wt with tCaMKII are comparable to those obtained with myc–GluK5DDD, indicating that this phospho-mimetic mutant represents a good approximation of GluK5 subunit phosphorylated by CaMKII.

The fact that CaMKII markedly promotes surface expression of GluK5-containing KARs may appear at odds with our initial observation that CaMKII is involved in the depression of synaptic KARs in a GluK5-dependent manner. We thus measured the amount of myc–GluK5 co-localized with Homer1C–GFP, a marker of postsynaptic densities, in dendritic spines of cultured hippocampal neurons (Figure 4D–F). Whereas the levels of myc–GluK5wt and myc–GluK5AAA were comparable, the levels of phospho-mimetic myc–GluK5DDD were markedly reduced at dendritic spines ($P<0.0001$) (Figure 4F). These results indicate that CaMKII-dependent phosphorylation of GluK5 increases surface expression of KARs at extrasynaptic sites, but decreases the number of synaptic GluK5-containing KARs at synaptic sites, in agreement with the KAR-LTD findings.

Phosphorylation of GluK5 increases lateral mobility of KARs

Because CaMKII-dependent phosphorylation of GluK5 decreased synaptic localization of KARs, we hypothesized that synaptic stability of KARs may be altered by CaMKII phosphorylation. To test that hypothesis we first examined the lateral mobility of HA-tagged GluK5wt and phospho-mutants using Quantum Dots (QDs) precoupled to anti-HA antibodies (QD–HA) (Figure 5A). As shown in Figure 5B and C, we found that phospho-mimetic HA–GluK5DDD presented an increased lateral mobility as compared with HA–GluK5wt ($P<0.0001$). On the contrary, we found that the non-phosphorylable mutant GluK5AAA displayed reduced lateral mobility ($P<0.0001$) (Figure 5B and C). To test whether CaMKII activation was sufficient to increase GluK5 mobility, we co-expressed constitutively active CaMKII and HA–GluK5. We found that CaMKII facilitated lateral diffusion of HA–GluK5wt ($P<0.0001$) but not that of phospho-mutants HA–GluK5AAA or HA–GluK5DDD (Figure 5D). The results suggest that CaMKII-mediated phosphorylation promotes the lateral escape of synaptic GluK5 receptors that may underlie the decreased content of KARs at synaptic sites.

CaMKII-dependent phosphorylation of GluK5 inhibits interaction with PSD-95

GluK2 and GluK5 bind PSD-95 through their C-terminal domain, playing a potential role in the stabilization of KARs at synaptic sites (Garcia *et al*, 1998). Binding of AMPARs to the scaffold PSD-95 promotes synaptic anchoring through a diffusion trap mechanism in a CaMKII-dependent manner (Bats *et al*, 2007; Opazo *et al*, 2010). We hypothesized that CaMKII-dependent phosphorylation of GluK5 may disrupt the interaction between KARs and PSD-95, promoting escape of GluK5 containing receptors from synapses via lateral diffusion. We thus investigated if CaMKII phosphorylation of GluK5 modified its ability to bind to PSD-95 (Figure 6). We performed GST-pulldown experiments between GST-GluK5 C-terminal domains (wt or mutants) and PSD-95 from brain extracts (Figure 6A). The binding of PSD-95 to GST-GluK5AAA was increased as compared with GluK5 ($P<0.05$), and was conversely decreased when incubated with the GST-GluK5DDD resins ($P<0.01$). We co-expressed myc–GluK5wt, myc–GluK5AAA or myc–GluK5DDD together with PSD-95 in COS-7 cells and performed co-immunoprecipitation experiments with an anti-myc antibody (Figure 6B). The relative amount of PSD-95 co-immunoprecipitated, as

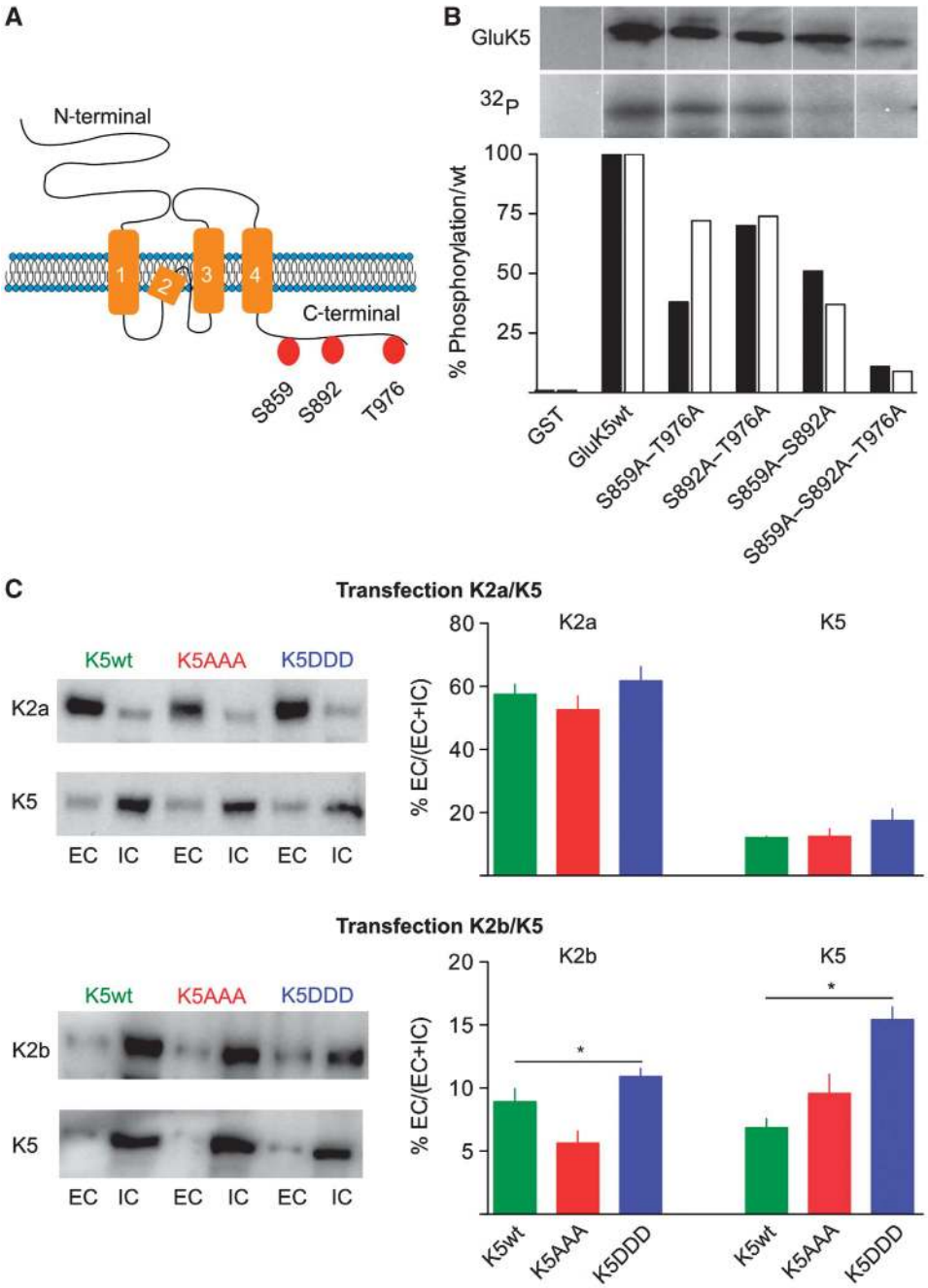

Figure 3 CaMKII phosphorylation sites in the GluK5 C-terminal domain and properties of GluK5 phosphorylation mutants. (**A**) Schematic representation of the GluK5 subunit, indicating the presence of three potential phosphorylation sites in the C-terminal domain of GluK5. (**B**) *In vitro* phosphorylation of GluK5 by CaMKII. GST fusion proteins (GST and GST-GluK5 WT or GST-GluK5 with point mutations in the C-terminal domain, as indicated) were phosphorylated with purified CaMKII *in vitro* using (γ-^{32}P) ATP and then exposed on an autoradiography film. The upper row represents total GluK5 protein loaded on the gel as revealed on western blots with an anti GluK5 antibody; the lower row represents autoradiograms of the corresponding gels. The original gel has been cropped for presentation purposes and can be found in the 'Source Data'. The histogram below represents relative levels of phosphorylation as compared with wt, for two individual experiments (the black bar corresponds to the gel illustrated). (**C**) Plasma membrane localization of GluK5wt and mutants in COS-7 cells. Biotinylation experiments in COS-7 cells transfected with the different mutants as indicated and with either HA–GluK2a or HA–GluK2b. Left panels: representative western blots probed with anti-HA antibodies to detect HA–GluK2 or with anti-myc antibodies to detect myc–GluK5 (EC, extracellular; IC, intracellular). Right panel: quantification of the western blots corresponds to the ratio between EC and total (EC + IC) receptors (myc–GluK5wt alone: 3.7 ± 0.5%, $n = 7$) (expression myc–GluK5 + HA–GluK2a: quantification for myc–GluK5: GluK5wt: 12.0 ± 0.4%, $n = 6$; GluK5AAA: 12.0 ± 2%, $n = 6$; GluK5DDD: 18.0 ± 3%, $n = 5$; quantification for HA–GluK2a: with GluK5wt: 57.5 ± 3.2%, $n = 3$; with GluK5AAA: 52.5 ± 4.4%, $n = 3$; with GluK5DDD: 61.7 ± 4.6%, $n = 3$) (expression myc–GluK5wt + HA–GluK2b: quantification for myc–GluK5: GluK5wt: 6.9 ± 0.7%, $n = 8$; GluK5AAA: 9.6 ± 1.5%, $n = 6$; GluK5DDD: 15.0 ± 1%, $n = 6$; quantification for HA–GluK2b: with GluK5wt: 8.9 ± 1%, $n = 4$; with GluK5AAA: 5.6 ± 1%, $n = 4$; with GluK5DDD: 10.9 ± 0.6%, $n = 4$). Data were compared using unpaired *t*-test ($^*P < 0.05$). Source data for this figure is available on the online supplementary information page.

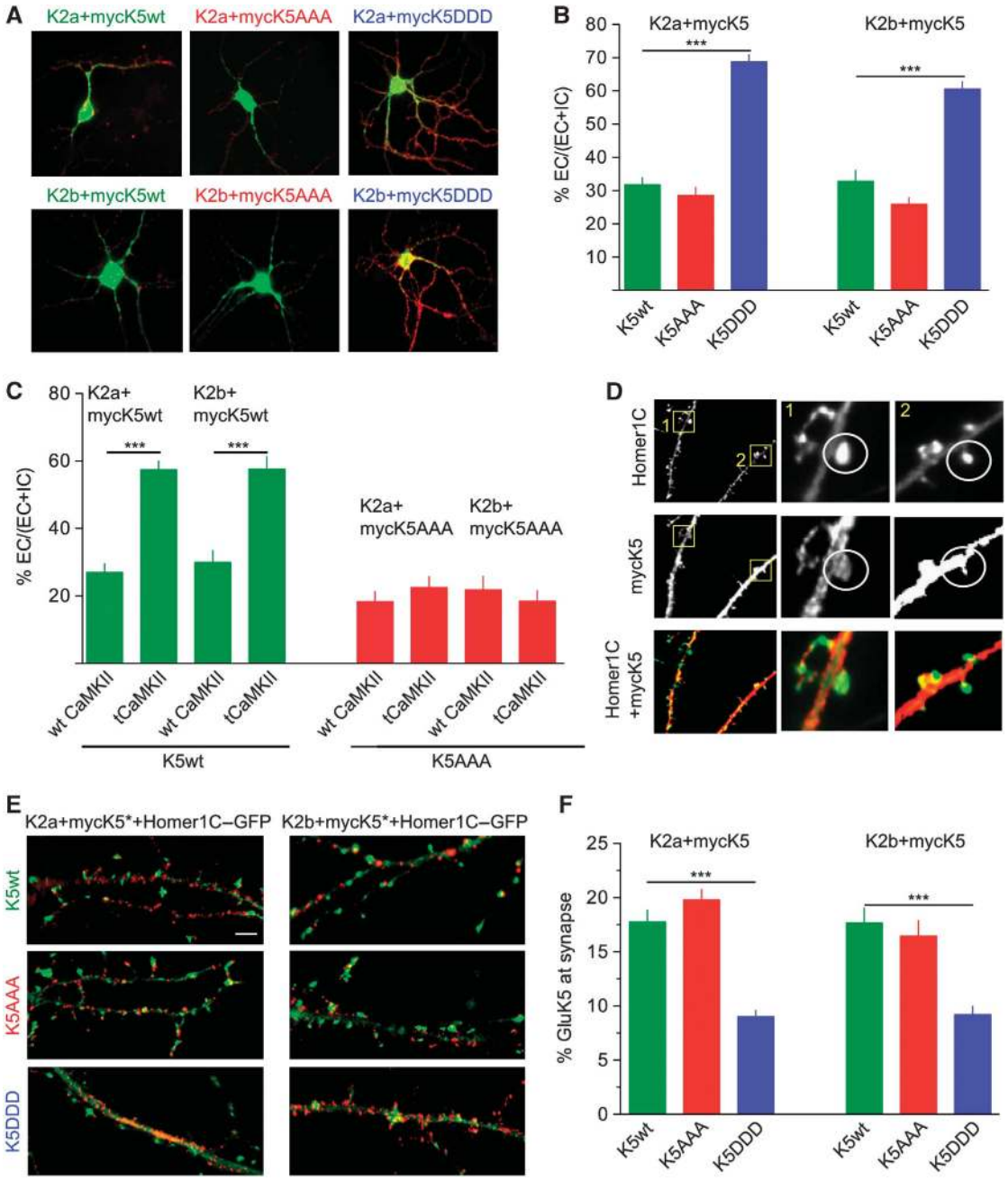

Figure 4 CaMKII phosphorylation increases expression of KARs at the plasma membrane of transfected hippocampal neurons and decreases their synaptic content. (**A**) Representative images of extracellular and total labelling of myc–GluK5 mutant proteins. Myc–GluK5wt, AAA or DDD were transfected with either GluK2a or GluK2b in mouse hippocampal neurons and expressed for 2 days. Secondary anti-rabbit Alexa Fluor-568 (red) labels extracellular GluK5-KARs and anti-mouse Alexa Fluor-488 (green) labels total receptors. (**B**) Quantification of the ratio between extracellular and total receptors (%EC/(EC + IC)) for neurons illustrated in (**A**) (myc–GluK5wt + GluK2a: 30 ± 2%, $n = 65$ cells; myc–GluK5DDD + GluK2a: 69 ± 3%, $n = 110$ cells; myc–GluK5AAA + GluK2a: 26 ± 3%, $n = 44$ cells; myc–GluK5wt + GluK2b: 34 ± 4%, $n = 31$ cells; myc–GluK5DDD + GluK2b: 61 ± 2%, $n = 84$ cells; myc–GluK5AAA + GluK2b: 25 ± 2%, $n = 65$ cells (three to five different experiments) (data were compared using unpaired *t*-test, $^{***}P < 0.001$). (**C**) Quantification of %EC/(EC + IC) for neurons co-expressing the different GluK5 heteromers as indicated, and wt or tCaMKII. (GluK2a + myc–GluK5wt + wt CaMKII: 27 ± 2.5%, $n = 29$; GluK2a + myc–GluK5wt + tCaMKII: 57 ± 3%, $n = 21$; GluK2b + myc–GluK5wt + wt CaMKII: 30 ± 3%, $n = 18$; GluK2b + myc–GluK5wt + tCaMKII: 58 ± 3%, $n = 14$) (GluK2a + myc–GluK5wt + wt CaMKII: 18 ± 3%, $n = 46$; GluK2a + myc–GluK5wt + tCaMKII: 22 ± 3%, $n = 36$; GluK2b + myc–GluK5wt + wt CaMKII: 21 ± 4%, $n = 28$; GluK2b + myc–GluK5wt + tCaMKII: 18 ± 3%, $n = 32$ (three and two experiments each) (data were compared using unpaired *t*-test, $^{***}P < 0.001$). (**D**) Characteristic images for the quantification of the co-localization between Homer1C (green) and GluK5 (red) in dendritic spines. (**E**) Representative images of extracellular myc–GluK5 mutant proteins and Homer1C–GFP for the different conditions as indicated in the figure. Scale bar represents 10 μm. (**F**) Quantification of myc–GluK5wt or myc–GluK5 mutants, as indicated, at synapses (identified as spiny structures of at least 15 pixels in size containing Homer1C–GFP staining). (myc–GluK5wt + GluK2a: 17.7 ± 1%, $n = 265$ synapses in 27 neurons; myc–GluK5DDD + GluK2a: 9 ± 1%, $n = 326$ synapses in 28 neurons; myc–GluK5AAA + GluK2a: 19.8 ± 1%, $n = 351$ synapses in 17 neurons; myc–GluK5wt + GluK2b: 17.7 ± 1%, $n = 212$ synapses in 10 neurons; GluK5DDD + GluK2b: 9.1 ± 1%, $n = 210$ synapses in 16 neurons; myc–GluK5AAA + GluK2b: 16.5 ± 1%, $n = 192$ synapses in 12 neurons, three experiments each). Data were compared using an unpaired *t*-test, $^{***}P < 0.0001$).

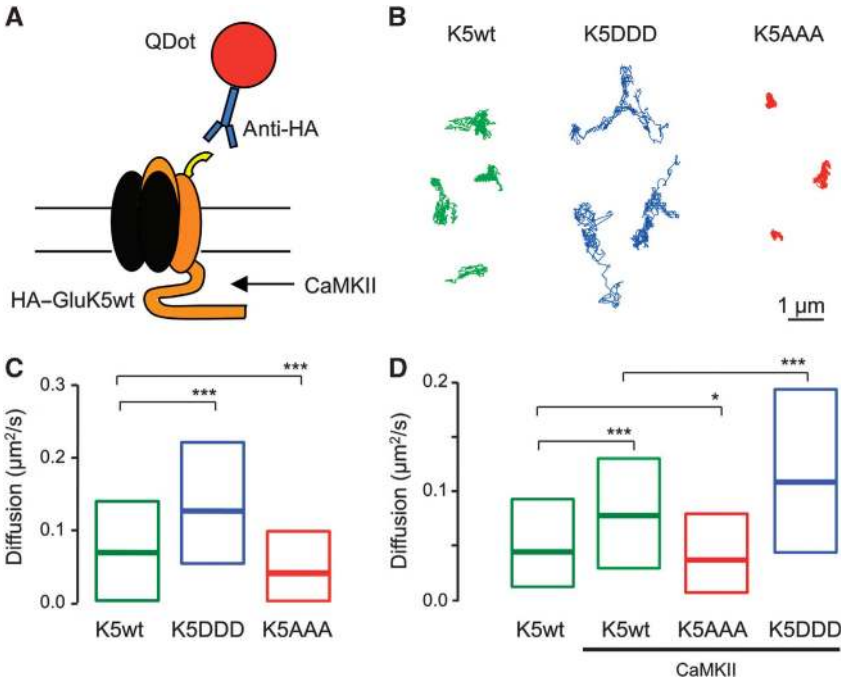

Figure 5 CaMKII phosphorylation increases the surface mobility of GluK5. (**A**) Schematic representation of the experimental manipulation. Recombinant HA–GluK5 receptors were exclusively tracked using QDots precoupled to HA antibodies. (**B**) Representative trajectories of the surface diffusion of recombinant GluK5wt (left), phospho-mimetic GluK5DDD (middle) and non-phosphorylable GluK5AAA (right). Note that mimicking phosphorylation dramatically increased the surface explored by HA–GluK5 during the recording period (30 s). Scale bar 1 μm. (**C**) Bar graph of the median diffusion (± 20–75% IQR) of QD-GluK5 WT or phosphor-mutants (median diffusion coefficient in $\mu m^2/s$: HA–GluK5wt 0.0654, $n = 1038$ QDs; HA–GluK5DDD 0.1223, $n = 2272$ QDs, HA–GluK5AAA 0.0371, $n = 998$ QDs. Mann–Whitney test $^{***}P < 0.001$). (**D**) Bar graph of the median diffusion (± 20–75% IQR) of QD-GluK5 receptors in the absence or presence of constitutively active CaMKII (T286D). Note that although active CaMKII phosphorylation increased the lateral diffusion of HA–GluK5, it did to a less extent than HA–GluK5DDD, suggesting that CaMKII only partially phosphorylate HA–GluKA5 (median diffusion coefficient in $\mu m^2/s$: HA–GluK5wt 0.0439, $n = 501$ QDs; HA–GluK5wt + active CaMKII 0.0774, $n = 562$ QDs; HA–GluK5AAA + active CaMKII 0.035, $n = 442$ QDs; HA–GluK5DDD + active CaMKII 0.1085, $n = 647$ QDs. Mann–Whitney test $^{*}P < 0.05$, $^{**}P < 0.01$, $^{***}P < 0.001$).

compared with myc–GluK5wt, was significantly higher with myc–GluK5AAA ($P < 0.01$) and lower with myc–GluK5DDD ($P < 0.0001$). These experiments indicate that CaMKII-dependent phosphorylation of GluK5 decreases interaction with PSD-95, and suggest that decreased binding of GluK5 to PSD-95 may be the mechanism by which KARs diffuse away from synaptic sites.

Role of CaMKII-dependent phosphorylation of GluK5 at mf-CA3 synapses

We directly addressed the consequences of CaMKII phosphorylation of GluK5 on KAR-EPSCs at mf-CA3 synapses using a molecular replacement strategy. In hippocampal slice cultures prepared from GluK5$^{-/-}$ (Figure 7A), we transfected CA3 pyramidal cells with either GluK5wt or phosphorylation mutants of GluK5 (Figure 7A and B). To compare different experimental conditions, the relative amplitude of KAR-EPSCs was measured with respect to the amplitude of AMPAR-EPSCs for each transfected cell recorded. The KAR/AMPAR EPSCs ratio was not significantly different in slices prepared from WT mice or from GluK5$^{-/-}$ mice (Figure 7C and D) while we found that KAR-EPSCs decayed significantly faster ($P < 0.01$) (Supplementary Figure S5A and B), as previously reported in acute slices (Sachidhanandam *et al*, 2009; Contractor *et al*, 2011).

CA3 pyramidal cells in slices prepared from GluK5$^{-/-}$ mice were transfected with either GluK5wt, GluK5DDD or GluK5AAA, together with GFP (Figure 7A and B). In neurons transfected with GluK5wt, the KAR/AMPAR ratio was not different from non-transfected neurons in GluK5$^{-/-}$ slices (Figure 7C and D). However, in neurons transfected with GluK5DDD, we found a significant reduction of the KAR/AMPAR ratio as compared with CA3 pyramidal cells recorded in WT, GluK5$^{-/-}$ slices or GluK5$^{-/-}$ slices transfected with GluK5wt ($P < 0.005$). Finally, in neurons transfected with GluK5AAA, the KAR/AMPAR ratio was not different from WT, GluK5$^{-/-}$ and GluK5$^{-/-}$ + GluK5wt conditions. The decay time constant after transfection with either GluK5wt, GluK5DDD or GluK5AAA recovered to values, which were not statistically different from that observed in WT slices, indicating that the transfected GluK5 was indeed incorporated into synaptic KARs (Supplementary Figure S5A and B). Our results show that incorporation of phospho-mimetic GluK5 (GluK5DDD) into native KARs significantly reduced KAR-EPSCs, suggesting that CaMKII-dependent phosphorylation of GluK5 directly decreases KAR-mediated transmission.

Phosphorylation of GluK5 is responsible for CaMKII-dependent STDP

Finally, we tested whether activation of endogenous CaMKII during the STDP protocol leads to synaptic depression of KAR-EPSCs by mechanisms that rely on the direct phosphorylation of GluK5. Neurons in slices prepared from GluK5$^{-/-}$ mice were transfected with either WT or mutated GluK5

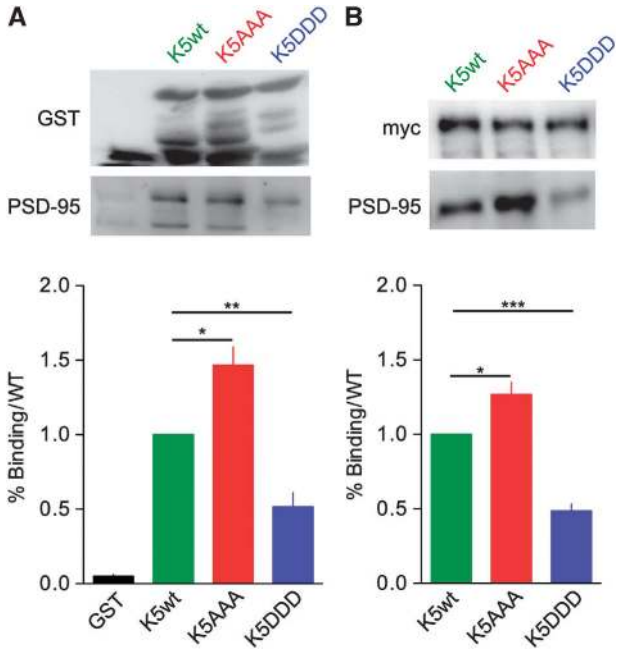

Figure 6 CaMKII phosphorylated form of GluK5 does not bind PSD-95. (**A**) GST pulldown of PSD-95 by the C-terminal domain of GluK5 mutants. Cytosolic extracts from mouse brain were incubated with the different GST fusion proteins as indicated. After binding and washes of the resins, samples were loaded on SDS gels and western blotted with an anti GST and anti-PSD-95. The amount of PSD-95 bound to each GST fusion proteins were normalized to the amount of PSD-95 bound to the C-terminal domain of GluK5wt. Data were compared using paired *t*-test ($n=5$ experiments, $^{*}P<0.05$, $^{**}P<0.01$). (**B**) Immunoprecipitation of PSD-95 by myc–GluK5wt and mutants expressed in COS-7 cells with an anti-myc antibody. Western blots were probed with anti-myc and anti-PSD-95 antibodies. Values are normalized to the amount of PSD-95 immunoprecipitated by the C-ter domain of GluK5wt. Data were compared using paired *t*-test ($n=9$ experiments, $^{*}P<0.01$, $^{***}P<0.0001$). Source data for this figure is available on the online supplementary information page.

subunits, in the attempt to rescue and occlude KAR-LTD. In slices prepared from GluK5$^{-/-}$, re-expression of GluK5wt restored KAR-LTD (Figure 8A and C) ($P<0.001$), confirming the crucial role of GluK5 for the expression of this form of synaptic plasticity. Interestingly, KAR-LTD was not observed in cells transfected with the phospho-null GluK5 mutant, GluK5AAA (Figure 8B and C). Finally, KAR-LTD was also absent in neurons transfected with the phospho-mimetic mutant GluK5DDD (Figure 8B and C). Although this result is consistent with an occlusion of KAR-LTD (KAR-EPSCs are already depressed), we cannot exclude that the absence of LTD with GluK5DDD is not linked with a decreased number of synaptic KARs, given the critical role of KARs activation in the induction of LTD. However, altogether these results indicate that CaMKII-dependent phosphorylation of GluK5 is necessary for spike-timing-dependent LTD of KARs at mf-CA3 synapses.

Discussion

This study reveals a novel mechanism by which CaMKII-dependent phosphorylation of the C-terminal domain of the GluK5 subunit leads to long-term depression of KAR-EPSCs. KAR-LTD operates through an original mechanism, which does not primarily rely on dynamin-dependent endocytosis, but rather on increased KAR mobility out of synaptic sites. Our data suggest that CaMKII-dependent phosphorylation of GluK5 results in unbinding of GluK5 from PSD-95 and subsequent untrapping of KARs from synaptic sites. Altogether, our results indicate opposing plasticity mechanisms for AMPARs versus KARs, and highlight the variety of mechanisms by which CaMKII regulates synaptic plasticity.

Activity-dependent plasticity of iGluRs at mf-CA3 synapses

Mf-CA3 synapses are known to exhibit presynaptic forms of plasticity expressed as an enhancement or a depression of glutamate release (Nicoll and Schmitz, 2005). Until recently, evidence for activity-dependent plasticity of AMPARs, NMDARs or KARs present at mf-CA3 synapses was lacking. NMDA receptors were recently found to be subject to LTP in an NMDA-dependent manner (Kwon and Castillo, 2008; Rebola *et al*, 2008). This LTP mediates a metaplastic switch making mf-CA3 synapses competent for the expression of NMDA-dependent LTP of AMPAR-EPSCs (Rebola *et al*, 2011). A conditioning activation of NMDARs depresses native KAR-mediated responses in a rapid and reversible manner (Ghetti and Heinemann, 2000), mediating a form of short-term plasticity of synaptic KARs (Rebola *et al*, 2007), and this depression depends on the activation of the phosphatase calcineurin which interacts with GluK2b (Coussen *et al*, 2005).

Here, we show that a pairing protocol known to induce CaMKII-dependent LTP of AMPA-EPSCs at other excitatory synapses, results in the selective LTD of KAR-EPSCs. Synaptic KARs can undergo LTD at mf-CA3 synapses, following stimulation for a period of 15–20 min while depolarizing CA3 pyramidal cells at $+30$ mV (Selak *et al*, 2009). This form of depression differed notably from KAR-LTD described here in its insensitivity to the Ca^{2+} chelator BAPTA, sensitivity to mGluR antagonists, and in the mechanism proposed. Recently, a comparable form of KAR-LTD dependent on mGluRs, but not on an intracellular rise of Ca^{2+} was described (Chamberlain *et al*, 2012). In contrast, KAR-LTD induced by the STDP-like protocol requires a rise in postsynaptic Ca^{2+} mainly mediated by voltage-gated Ca^{2+} channels, is insensitive to mGluR antagonists, and does not primarily involve dynamin-dependent endocytosis. A possible explanation for the different induction mechanisms may rely on the fact that the STDP-like protocol used favours activation of L-type Ca^{2+} channels, through short repeated depolarization pulses. Interestingly, KAR-LTD does not depend on the activation of NMDARs, but requires the activation of synaptic KARs. KARs could play a role by increasing Ca^{2+} influx, an ionotropic mechanism that could be amplified by the summation properties of KAR-EPSCs during burst stimulation. Alternatively, synaptic KARs involved in metabotropic signalling (Melyan *et al*, 2004; Ruiz *et al*, 2005) may regulate their number at the cell membrane, as in neuroblastoma cells (Rivera *et al*, 2007).

This is the first example of activity-dependent plasticity of synaptic KARs mediated by activation of CaMKII. Interestingly, CaMKII activation appears to exert opposite regulation on two types of glutamate receptors, by depressing synaptic KARs and potentiating synaptic AMPARs, even

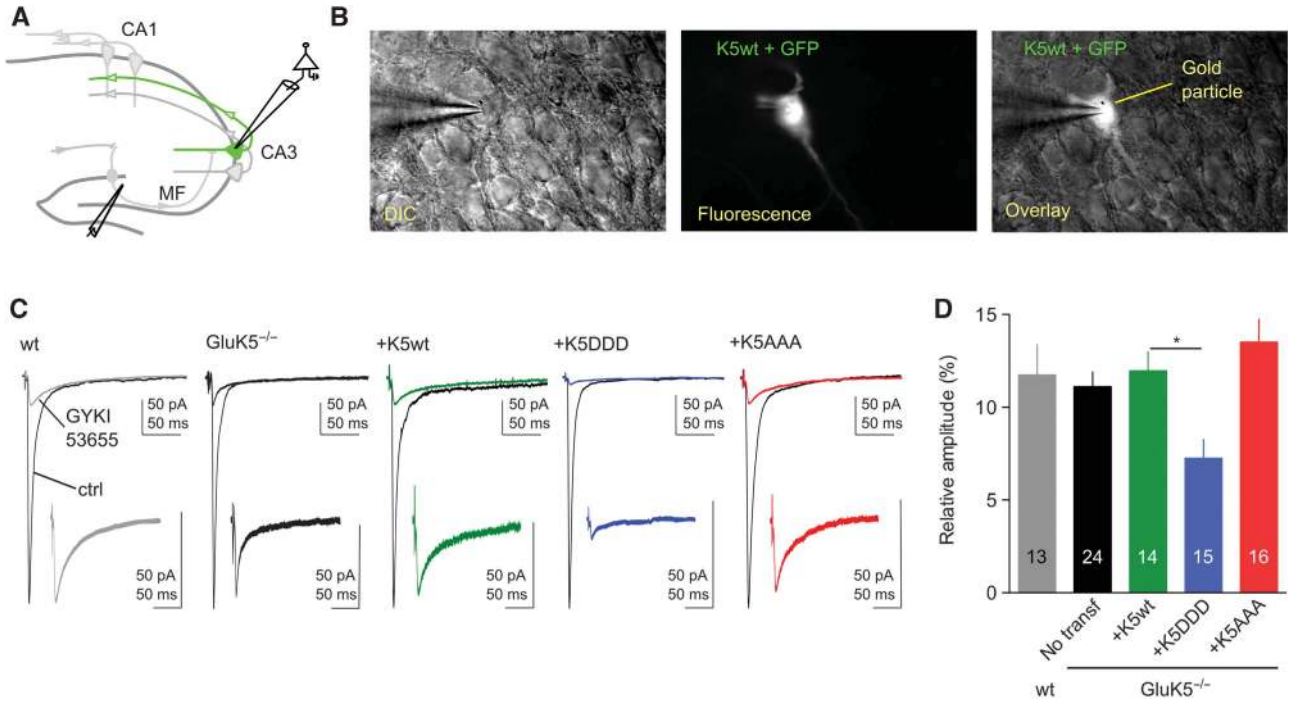

Figure 7 CaMKII-dependent phosphorylation of GluK5 regulates synaptic KARs. (**A**) Schematic cartoon of the hippocampus illustrating a cell co-transfected with GFP and the gene of interest. (**B**) Example images of a CA3 pyramidal cell co-transfected with GFP and GluK5wt. (**C**) Voltage-clamp recordings were performed on GFP-expressing pyramidal cells at −70 mV in the presence of bicuculline (10 μM), D-AP5 (50 μM) and a low concentration of NBQX (150 nM) to limit polysynaptic activity. In all, 30 responses evoked at 3 Hz were averaged in the absence and in the presence of 50 μM GYKI53655, to isolate the AMPAR and the KAR component of the mf-CA3 synaptic response, respectively. In the insert are showed enlargements, by the same proportion, of isolated KAR-EPSCs. (**D**) Summary of the results of the relative amplitude of KAR-EPSCs versus AMPAR-EPSCs after transfection with either WT or mutated GluK5 subunits (wt: 11.8 ± 1.4%, $n = 13$; GluK5$^{-/-}$: 11.1 ± 0.8%, $n = 24$; GluK5$^{-/-}$ + GluK5wt: 11.9 ± 1.0%, $n = 14$; GluK5$^{-/-}$ + GluK5DDD: 7.2 ± 0.9%, $n = 15$; GluK5$^{-/-}$ + GluK5AAA: 13.5 ± 1.2%, $n = 16$). Values are presented as mean ± s.e.m. of n experiments. Data were compared using one-way ANOVA followed by Dunnett's multiple comparison test (*$P < 0.005$).

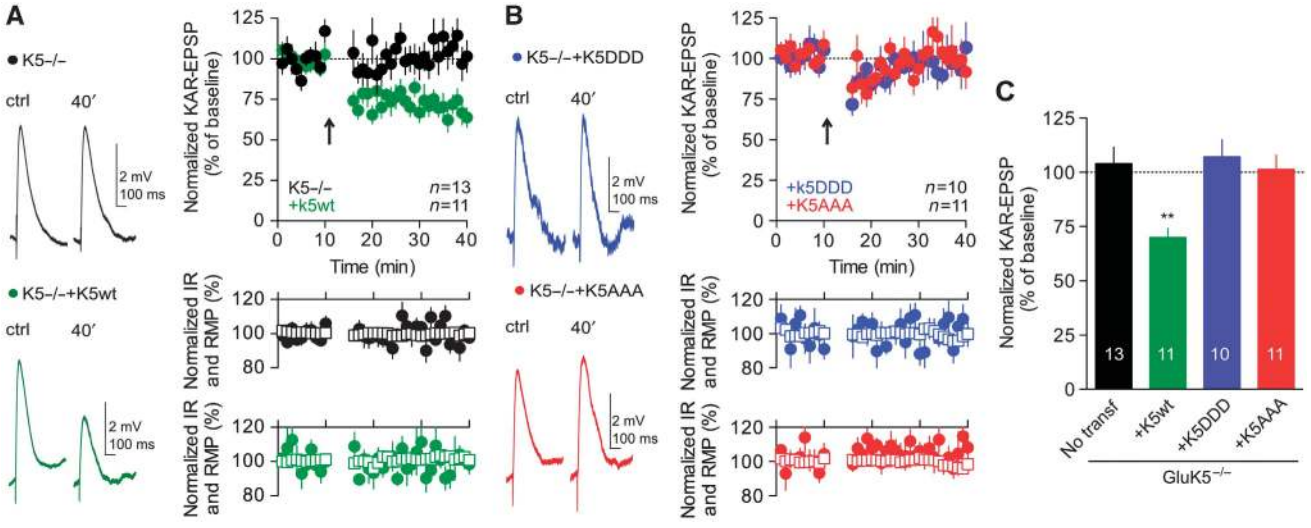

Figure 8 Phosphorylation of GluK5 is responsible for CaMKII-dependent KAR-LTD. (**A**) In slices prepared from GluK5$^{-/-}$ mice, re-expression of GluK5wt restored KAR-LTD. Representative traces of current-clamp recordings of KAR-EPSPs before and after the pairing protocol, in GluK5$^{-/-}$ and after transfection with GluK5wt. Input resistance (empty squares) and resting membrane potential (filled circles) remained stable throughout the experiment. (**B**) KAR-LTD was not observed in cells transfected with the GluK5DDD or GluK5AAA. Representative traces of KAR-EPSPs before and after the pairing protocol, after transfection with GluK5DDD or GluK5AAA. (**C**) Summary of the changes of KAR-EPSP amplitudes after STDP-like protocol in slices prepared from GluK5$^{-/-}$ mice, and after transfection with WT or mutated GluK5 subunit (GluK5$^{-/-}$: 104.1 ± 7.5%, $n = 13$; GluK5$^{-/-}$ + GluK5wt: 69.9 ± 4.3%, $n = 11$; GluK5$^{-/-}$ + GluK5DDD: 107.2 ± 7.9%, $n = 10$; GluK5$^{-/-}$ + GluK5AAA: 101.4 ± 6.5%, $n = 11$). Values are presented as mean ± s.e.m. of n experiments. Data were compared using unpaired t-test (**$P < 0.001$).

though this has not yet been demonstrated at mf-CA3 synapses. A role for CaMKII in mediating LTD of AMPA-EPSCs was observed at cerebellar parallel fibre-Purkinje cell synapses (Hansel *et al*, 2006), although several other kinases are also involved and the mechanism of action of CaMKII is not known.

The C-terminal tail of the GluK2 subunit of KARs can be phosphorylated by PKA inducing potentiation of whole-cell currents (Kornreich *et al*, 2007) and markedly altering trafficking and endocytosis of KARs in cell culture systems (Nasu-Nishimura *et al*, 2010). PKC activation regulates KAR trafficking to the membrane (Hirbec *et al*, 2003; Martin and Henley, 2004; Rivera *et al*, 2007) and is involved in activity-dependent synaptic depression of KARs (Park *et al*, 2006; Martin *et al*, 2007; Selak *et al*, 2009; Chamberlain *et al*, 2012). Phosphorylation of the C-terminal domain of GluK2 promotes GluK2 SUMOylation, which is required for the internalization of GluK2-containing KARs that occurs during mGluR-dependent KAR-LTD (Chamberlain *et al*, 2012). Although KAR-LTD induced by the STDP-like protocol is also blocked by PKC inhibitors, the mechanisms are likely to be different, in particular because it does not primarily depend on internalization of KARs. Possibly, PKC may be involved in the activation of CaMKII itself as previously reported (Yan *et al*, 2011).

CaMKII-dependent phosphorylation of GluK5

Contrary to KARs, it has long been known that AMPARs are themselves primary targets of CaMKII. However, whereas GluA1 can be phosphorylated by CaMKII during induction of LTP at Ser831 (Barria *et al*, 1997) leading to increased conductance, this does not suffice to explain persistent synaptic changes, which likely rely on increased number of synaptic receptors (Derkach *et al*, 2007; Lee *et al*, 2010). Here, we provide the first evidence that GluK5, which stands as a key KAR subunit for LTD can be phosphorylated by CaMKII on three identified residues in the C-terminal domain. We show that phosphorylation of GluK5 by CaMKII leads to increased surface expression of GluK5-containing KARs in cultured hippocampal neurons, when expressed with either GluK2a or GluK2b. The expression of phospho-null GluK5 yields either no or only small changes as compared with GluK5wt (in cultured neurons; as well as in slices, see below) suggesting that in basal conditions the level of KARs phosphorylated by CaMKII is low.

Regulated lateral mobility of KARs

Increased surface expression of KARs upon CaMKII-dependent phosphorylation may appear in contradiction with a role of CaMKII in the LTD of synaptic KARs. We propose an explanation for this apparent contradiction by providing evidence that CaMKII-dependent phosphorylation also promotes decreased synaptic content of KARs, likely by untrapping KARs from synaptic sites. This would explain the observed decrease in the content of GluK5DDD-KARs at synaptic sites in cultured hippocampal neurons, and the decreased amplitude of KAR-EPSCs upon re-expression of GluK5DDD in slice cultures prepared from GluK5$^{-/-}$ mice. Using single-particle tracking of HA-tagged GluK5-containing receptors in cultured hippocampal neurons, expressing or not tCaMKII (Opazo *et al*, 2010), we showed that activation of CaMKII leads to a marked increase in the lateral mobility of GluK5-containing KARs. This increased lateral mobility was reproduced by expression of the phospho-mimetic GluK5 mutant but not the phospho-null GluK5, indicating that it is a consequence of the direct phosphorylation of GluK5. Hence, upon CaMKII-dependent phosphorylation, GluK5-containing KARs appear to diffuse away from synaptic sites.

In striking contrast, CaMKII activation induces synaptic trapping of AMPARs diffusing in the membrane (Opazo *et al*, 2010). Interaction of stargazin with AMPAR subunits is essential for delivering functional receptors to the plasma membrane, whereas its binding with PSD-95 is required for targeting the AMPARs to the synapse (Chen *et al*, 2000; Bats *et al*, 2007). AMPARs and stargazin diffuse as complexes in both the synaptic and extrasynaptic plasma membrane (Bats *et al*, 2007). These complexes are trapped reversibly at synapses through CaMKII-dependent phosphorylation of stargazin resulting in the binding to PSD-95 (Opazo *et al*, 2010). We propose that a converse situation may exist for KARs, whereby CaMKII-dependent phosphorylation releases KAR binding from PSD-95. We confirmed that GluK5 directly binds PSD-95 (Garcia *et al*, 1998) and we found that CaMKII-dependent phosphorylation of GluK5 markedly inhibits this interaction. The phosphorylation sites are not necessarily directly involved in the binding of PSD-95, and CaMKII-dependent phosphorylation of GluK5 may be inducing changes in the folding of the C-ter domain of GluK5, making the PSD-95 binding sites less accessible. Hence, our results suggest that, contrary to AMPARs, CaMKII-dependent phosphorylation of GluK5 results in unbinding of KARs from the postsynaptic scaffold protein PSD-95, leading to untrapping from synaptic sites. Altogether, our results provide the first evidence for the regulated lateral mobility of KARs and point to a role of PSD-95 in the trapping of KARs at synaptic sites.

Mechanisms of KAR-LTD at mf-CA3

The molecular replacement strategy used here, which consists in the re-expression of WT or mutated GluK5 on a GluK5$^{-/-}$ background in hippocampal slice cultures, has proven to be very valuable. Re-expression of the phospho-mimetic GluK5DDD leads to a decrease in the amplitude of KAR-EPSCs, whereas re-expression of the phospho-null GluK5AAA subunit was without any effect. This cannot be accounted by changes in the biophysical properties of GluK2/GluK5DDD KARs, which were found to be identical to those of GluK2/GluK5 in heterologous cells (Supplementary Figure S4). Hence, CaMKII-dependent phosphorylation of GluK5 decreases synaptic content of KARs at mf-CA3 synapses, as shown in cultured hippocampal neurons. Moreover, the phospho-null GluK5 mutant prevented KAR-LTD of KAR-EPSPs at mf-CA3 synapses, indicating that CaMKII-dependent phosphorylation of GluK5 was required for KAR-LTD.

There is mounting evidence for a variety of mechanisms for synaptic plasticity. Here, we uncovered an original mechanism for LTD of KARs relying on activation of KARs, postsynaptic Ca^{2+} influx through voltage-gated Ca^{2+} channels, and activation of CaMKII leading to phosphorylation of GluK5 (Supplementary Figure S6). The proposed mechanism for KAR-LTD involves untrapping of KARs from the PSD and diffusion away from synaptic sites, but does not primarily rely on internalization mechanisms. Indeed, infusion in the patch pipette of D15 or dynasore, to block dynamin-dependent

endocytosis, was without any effect on KAR-LTD. In contrast, LTD of KAR-EPSCs induced by prolonged depolarization and/or 1 Hz stimulation (Selak *et al*, 2009) is independent of postsynaptic Ca^{2+} influx and depends on internalization of KARs. KAR-LTD also differs from NMDAR-dependent LTD in the CA1 region of the hippocampus, which is known to require a Ca^{2+}-dependent internalization of AMPARs (Carroll *et al*, 2001). LTD of KARs induced by the STDP-like protocol thus appears to be mediated by very distinct mechanisms. Overall, it is tempting to speculate that the opposite control of AMPARs and KARs following coordinated pre- and postsynaptic activity, as with the STDP protocol, may lead to the modulation in the temporal integration properties of mf-CA3 synapses.

Materials and methods

DNA constructs

cDNAs coding for the rat GluK5 were inserted into the expression vector pcDNA3, tagged with six consecutive myc epitopes or with an HA tag after the signal sequence for WT GluK5 (myc–GluK5wt), phosphorylation mutants (myc–GluK5AAA and myc–GluK5DDD). Site-directed mutagenesis was performed using Quick Exchange XL kit (Stratagene, The Netherlands). cDNAs were sequenced and expressed in COS-7 cells to verify molecular weight by western blot analysis with the anti GluK5 C-terminus antibody. GluK2 cDNA were described previously (Coussen *et al*, 2005).

GST-pulldown assay and in vitro phosphorylation

cDNAs encoding the rat C-terminal GluK5 subunit (starting at the amino acid 826) was subcloned into pGex-4T-1 vector (Amersham Biosciences) and subject to directed mutagenesis. Proteins were produced and purified as previously described (Coussen *et al*, 2002). For phosphorylation assays, proteins were cut for 2 h with glutathion and the unbound fraction was collected for the reaction. CaMKII phosphorylation was performed as recommended by the manufacturer (Biolab). Samples were run on SDS gels, blotted on nitrocellulose and exposed on Kodak films for 3 days. Nitrocellulose filters were blotted with anti-GluK5 antibodies. Images were taken and analysed with a Syngene apparatus. Statistical analyses were made with PRISM using paired *t*-test.

Electrophysiology experiments

HEK293 cells. Cells were transfected using FUGENE 6 with GFP, GluK2a(Q) or GluK2b(Q). To study whether basic electrophysiological properties of GluK2/GluK5 heteromeric receptors are modified by the phosphorylation of the GluK5 subunit, GFP and GluK2 cDNAs were co-transfected with GluK5wt, GluK5AAA or GluK5DDD at a ratio of 1:1:5 in order to favour the expression of GluK2/GluK5 heteromers over GluK2 homomers (Barberis *et al*, 2008). Two days after transfection, cells were bathed in Hepes-buffered solution (HBS) containing (in mM): 145 NaCl, 2 KCl, 2 $MgCl_2$, 2 $CaCl_2$, 10 glucose, and 10 Hepes, adjusted to 320 mOsm per liter and pH 7.4 with NaOH, at room temperature. Whole-cell recordings were performed 2 days after transfection. Green fluorescent cells lifted off the coverslip, placed under the flow of a theta tube and held at -80 to -40 mV. Recording pipettes (resistance 4–6 MΩ) were filled with a solution containing (in mM): 130 $CsCH_3SO_3$, 2 NaCl, 2 $MgCl_2$, 10 EGTA, 10 HEPES, 4 Na_2ATP, 0.1 spermine, adjusted to 310 mOsm per liter and pH 7.2 with CsOH. Currents were evoked by long application of 1 mM glutamate for 100 ms every 20 s by moving the theta tube laterally with a piezoelectric device, under computer control. The decaying phase of the currents was fitted with a function in the following form: $y(t) = \Sigma A_i \exp(-t/\tau_i)$, where A_i are the fractions of respective components ($\Sigma A_i = 1$) and τ_i are the time constants. In double-exponential fits, the weighted deactivation time constant τ_w was calculated using the formula $\tau_w = \Sigma A_i\ \tau_i$. A maximum of two exponential components were used (Barberis *et al*, 2008).

Slice culture preparation and transfection; acute slice preparation. Organotypic hippocampal slice cultures were prepared from P5–P8 C57BL6 WT and GluK5$^{-/-}$ mice as described previously (Stoppini *et al*, 1991) according to the guidelines of the University of Bordeaux/CNRS Animal Care and Use Committee. Three to four days after plating, the medium was replaced and then changed every 2–3 days. We used the Helios gene gun device (Bio-Rad) with modified barrel (O'Brien and Lummis, 2006) to co-transfect individual cells with cDNAs encoding soluble GFP and WT or mutated GluK5. 8 mg colloidal gold (1.6 μm, Bio-Rad) was coated with 20 mg of each co-transfected construct. Electrophysiological experiments were performed after 6–10 days in culture and 2–4 days after transfection. For acute slices recordings, transverse hippocampal slices (320 mm thick) were obtained from 17- to 19-day-old C57Bl/6 WT and GluK5$^{-/-}$ mice killed by cervical dislocation.

Electrophysiological recordings in slice. Whole-cell voltage-clamp recordings (3.5–4.5 MΩ electrodes) were made at 30–32°C from CA3 pyramidal cells visualized by infrared videomicroscopy. Transfected cells were recognized by the GFP fluorescence. Slices were perfused with an extracellular solution composed of 125 mM NaCl, 2.5 mM KCl, 1.25 mM NaH_2PO_4, 26 mM $NaHCO_3$, 2.3 mM $CaCl_2$, 1.3 mM $MgCl_2$ and 25 mM glucose saturated with 95% O2/5% CO_2. Bicuculline (10 μM) was added to the bath to block $GABA_A$ receptors. For slice culture recordings, low concentration of NBQX (150 nM) was constantly present in the extracellular solution to decrease polysynaptic activity. The intracellular solution was composed of: 140 mM potassium methanesulfonate, 2 mM MgCl2, 4 mM NaCl, 5 mM phospho-creatine, 2 mM Na2ATP, 10 mM EGTA, 10 mM HEPES, 0.33 mM GTP (pH 7.3). In voltage-clamp experiments, potassium methanesulfonate was substituted by an equivalent concentration of caesium methanesulfonate. Mossy fibre (mf) synaptic responses were evoked by minimal stimulation (Marchal and Mulle, 2004) by placing a patch pipette filled with ACSF in the dentate gyrus. Synaptic currents were first identified in the voltage-clamp mode before switching to current-clamp according to the following criteria: low release probability at 0.1 Hz, marked low–frequency facilitation, rapid single rise times (Supplementary Figure S1A and B) and sensitivity to the group 2/3 mGluR agonist LCCG-1 [(2S,1S,2S)-2-(carboxycyclopropyl)glycine] (10 μM). The resting membrane potential of CA3 pyramidal cells ranged between -68 and -75 mV. If necessary, a small negative current ($\sim$10/50 pA) was injected into the postsynaptic cell to adjust membrane potential between -70 and 75 mV. Input resistance was monitored with small current steps (-20 pA for 300 ms) and cells were excluded if changed by >20%. During plasticity experiment, in order to better study the amplitude of synaptic KAR-mediated response, we activated mf-CA3 synapses every 30 s using a stimulating protocol that consist of three stimuli (delivered with 40 ms of interval) followed by a single fourth stimulus delivered after 480 ms. We use the amplitude of the response to the last stimulation (the fourth) to measure plasticity (Supplementary Figure S2A). A spike-timing-dependent-plasticity like protocol was induced by pairing three presynaptic stimulations (20-ms interval) with three postsynaptic action potentials (20-ms interval) triggered 10 ms after the presynaptic stimulations. This pairing was repeated 100 times every 3 s. Inverse pairing consisted of an identical protocol to the one described above, but with the three postsynaptic action potentials (20-ms interval) preceding by 10 ms the 3 presynaptic stimulations (20-ms interval). Measurements of KAR-LTD made in voltage-clamp mode were done using the K-based intracellular solution. The induction protocol was applied in current clamp. KAR-mediated synaptic currents were best fitted using a double exponential. To accurately report the KAR decay time constant (tau), a weighted tau was calculated as previously described (Rumbaugh and Vicini, 1999) using the following formula: $\tau_W = \tau_F[I_F/(I_F + I_S)] + \tau_S[I_S(I_F + I_S)]$, where I is the current amplitude, I_F and I_S are the peak amplitudes of the fast and slow components, respectively, and τ_F and τ_S are the respective time constants. LTD at Schaffer collateral-CA1 synapses experiment were performed in slice culture in the presence of N^6-cyclopentyladenosine (50–100 nM) to reduce polysynaptic activity. LTD was induced by 900 stimulation pulses at 1 Hz for while holding cells at -40 mV, using a Cs-based intracellular solution containing Qx314 5 mM (Supplementary Figure S3F). Small, hyperpolarizing voltage/current steps were given before each afferent stimulus allowing on-line monitoring of input and series resistance. The access resistance was <20 MΩ, and cells were discarded if it changed by >20%. No

series resistance compensation was used. Recordings were made using an EPC 10 amplifier (HEKA Elektronik, Lambrecht/Pfalz, Germany) and were filtered at 0.5–1 kHz, digitized at 5 kHz, and stored on a personal computer for additional analysis (IGOR PRO 5.0; WaveMetrics, Lake Oswego, OR). Values are presented as mean ± s.e.m. Either a paired or unpaired Student's *t*-test was used to define statistical differences between values.

Immunocytochemistry. Primary cultures of hippocampal neurons from WT mice were performed as in Jaskolski *et al* (2004). After 8 days *in vitro*, neurons were transfected with myc–GluK5 cDNAs as indicated in the figures, either alone or with GluK2a or GluK2b. Double labelling of extra- versus intracellular proteins was performed as in Jaskolski *et al* (2004). For co-localization with Homer1C, myc–GluK5wt, GluK2a/b and Homer1C–GFP were transfected in hippocampal neurons after 10 days *in vitro*. Immunocytochemistry was performed at 14 days *in vitro*. Extracellular labelling of myc–GluK5wt was performed with the polyclonal anti-myc antibody (1/500) on live neurons. Neurons were then fixed with paraformaldehyde and the second anti-rabbit Alexa Fluor-588 antibody was added. Green images correspond to expression of Homer1C–GFP. Immunofluorescence was visualized with an up-right epifluorescence microscope (Leica Microsystems, Wetzlar, Germany). Image acquisition was performed with a LEICA camera and the Metamorph analysis software.

Co-localization images were analysed with the MATLAB software as in Jaskolski *et al* (2005). To compute the degree of apposition between expressed myc–GluK5wt and postsynaptic clusters (Homer1c–GFP), a plug-in was developed on Metamorph software. Fifteen pixels regions corresponding to synapses (green from Homer1C–GFP and spiny shape) were selected on the images, allowing identification of synaptic structures as individual objects. The number of red pixels co-localized within the corresponding region was calculated as the percentage over the threshold area. These apposed regions were used to determine the percentage of synaptic GluK5 subunit. All the statistical analyses were made with PRISM using unpaired *t*-test.

Mobility experiments

GluK5 receptor labelling. QDs 655 goat *F*(*ab*')2 anti-rat IgG Conjugate (H + L) were from Invitrogen Corporation. HA–GluK5 WT and mutants were labelled by using QDs precoated with rat anti-HA antibodies (3F10, Roche). QDs (0.1 μM) were incubated with 1 μg AB in 10 μl PBS for 30 min. Non-specific binding was blocked by adding casein to the precoated QDs 15 min before use. We then incubated rat dissociated cultured hippocampal neurons (E18 from Sprague-Dawley rats) with precoated QDs (final dilution 0.5 nM) for 10 min at 37°C in culture medium. This incubation was followed by four washing steps, 30 s each. All washes were performed in ECS (extracellular solution; NaCl 145 mM, KCl 5 mM, Glucose 10 mM, Hepes 10 mM, $CaCl_2$ 2 mM and $MgCl_2$ 2 mM) supplemented with BSA 2%. After washing, neurons were mounted in an open chamber (Warner Instruments) and imaged in ECS.

Single-particle imaging. Cells were imaged at 35–37°C on an inverted epifluorescence microscope equipped with a 100× objective (NA = 1.3). QDs were detected by using a mercury lamp (excitation filter 560RDF55 or 460BP40 and emission filters 655WB20 or 655WB40). Fluorescent images from QDs were obtained with an integration time of 50 ms with up to 1200 consecutive frames. Signals were recorded with a back-illuminated thinned CCD97 camera (Photometrics Cascade 512B, Roper Scientific). QD-labelled GluK5 were imaged on randomly selected dendritic regions over up to a total experimental time of 30 min. QDs fixed on the cover slip allowed us to compensate for mechanical drifts of the stage.

Receptor tracking and analysis. The tracking of single QDs was performed with homemade software based on Matlab (Mathworks Inc., Natick, USA). Single QDs were identified by their blinking fluorescent emission and their diffraction-limited signals. Owning to the random blinking events of the QDs, the trajectory of a QD tagged receptor could not be tracked continuously. Subtrajectories of the same receptor were reconnected when the positions before and after the dark period were compatible with borders set for maximal position changes between consecutive frames and blinking rates. The values were determined empirically: 2–3 pixels (0.32–0.48 mm) for maximal position change between two frames and maximal dark periods of 25 frames (1.25 s). Mean square displacement (MSD) curves were calculated for reconnected trajectories of at least 75 frames. The QDs were considered synaptic if co-localized with clusters of the synaptic marker Homer1c∑GFP for at least five frames. Diffusion coefficients were calculated by a linear fit of the first 4–8 points of the MSD plots versus time depending on the length of the trajectory within a certain compartment. The resolution limit for diffusion was 0.0075 $\mu m^2/s$ whereas the localization precision was ∼40 nm. Statistical values are given as medians ± 25%/75% interval. Statistical significances were performed by using GraphPad Prism software. Non-Gaussian distributed data sets were tested by Mann–Whitney *t*-test. Indications of significance correspond to *P*-values <0.05 (*), $P<0.005$ (**) and $P<0.0005$ (***).

Antibodies and reagents

Primary antibodies. Monoclonal anti-myc (9E10) and rat anti-HA (3F10), Roche; polyclonal anti-myc, anti-KA2 (GluK5) and anti-R6R7NL9 (GluK2/3), Upstate Biotechnology; polyclonal anti-GFP, Molecular Probes; monoclonal anti-HA, Covance. Secondary antibodies: Alexa Fluor-568 goat anti-rabbit, Alexa Fluor-568 goat anti-mouse and Alexa Fluor-488 anti-mouse, Molecular Probes. For western blots, secondary peroxydase labelled antibodies, P.A.R.I.S Biotechnology. All drugs were obtained from Tocris Bioscience (Ballwin, MO), Sigma (St Louis, MO) or Ascent Scientific (Bristol, UK).

For lateral mobility experiments and for experiments which involved mutant mice or re-expression of cDNA constructs in slices, approximately one-half of experiments were done and analysed blind with respect to construct expressed or to the genotype of the mice. Results were similar and thus pooled with non-blind results.

Supplementary data

Supplementary data are available at *The EMBO Journal* Online (http://www.embojournal.org).

Acknowledgements

This study was supported by the Centre National de la Recherche Scientifique, the Conseil Régional d'Aquitaine, the European Commission (EUSynapse Project, contract no. LSHM-CT-2005-019055; EIF Fellowship awarded to MC; IIF Fellowship awarded to PO and ERC Grant 232942 Nano-Dyn-Syn to DC) and the Agence Nationale de la Recherche (contract MossyGlu). We thank Jessica Ragues for producing the plasmid DNAs, Elisabeth Normand, Alice Vimeney, Noelle Grosjean and Audrey Lacquement for taking care of the mice and for neuronal cultures. Confocal microscopy was performed at the Bordeaux Imaging Center. The help of Philippe Legros, Christel Poujol and Laure Malicieux is acknowledged. We thank Nelson Rebola and all members of the Mulle lab for suggestions and discussions.

Author contributions: Mario Carta performed and analysed all slice electrophysiology experiments in combination with pharmacological and molecular replacement approaches; Patrizio Opazo performed and analysed the lateral mobility experiments, Julien Veran performed the electrophysiological analysis of recombinantly expressed receptors in HEK 293 cells, Axel Athané helped with the production of cDNA constructs, Daniel Choquet helped with the design and analysis of the lateral mobility experiments, Françoise Coussen designed and performed the biochemical and cell biological experiments, and co-supervised the project, Christophe Mulle supervised the project and wrote the manuscript together with MC and FC.

Conflict of interest

The authors declare that they have no conflict of interest.

References

Barberis A, Sachidhanandam S, Mulle C (2008) GluR6/KA2 kainate receptors mediate slow-deactivating currents. *J Neurosci* **28:** 6402–6406

Barria A, Muller D, Derkach V, Griffith LC, Soderling TR (1997) Regulatory phosphorylation of AMPA-type glutamate receptors by CaM-KII during long-term potentiation. *Science* **276:** 2042–2045

Bats C, Groc L, Choquet D (2007) The interaction between Stargazin and PSD-95 regulates AMPA receptor surface trafficking. *Neuron* **53:** 719–734

Caporale N, Dan Y (2008) Spike timing-dependent plasticity: a Hebbian learning rule. *Annu Rev Neurosci* **31:** 25–46

Carroll RC, Beattie EC, von Zastrow M, Malenka RC (2001) Role of AMPA receptor endocytosis in synaptic plasticity. *Nat Rev Neurosci* **2:** 315–324

Chamberlain SE, Gonzalez-Gonzalez IM, Wilkinson KA, Konopacki FA, Kantamneni S, Henley JM, Mellor JR (2012) SUMOylation and phosphorylation of GluK2 regulate kainate receptor trafficking and synaptic plasticity. *Nat Neurosci* **15:** 845–852

Chen L, Chetkovich DM, Petralia RS, Sweeney NT, Kawasaki Y, Wenthold RJ, Bredt DS, Nicoll RA (2000) Stargazin regulates synaptic targeting of AMPA receptors by two distinct mechanisms. *Nature* **408:** 936–943

Contractor A, Mulle C, Swanson GT (2011) Kainate receptors coming of age: milestones of two decades of research. *Trends Neurosci* **34:** 154–163

Contractor A, Sailer AW, Darstein M, Maron C, Xu J, Swanson GT, Heinemann SF (2003) Loss of kainate receptor-mediated heterosynaptic facilitation of mossy-fiber synapses in KA2 $-/-$ mice. *J Neurosci* **23:** 422–429

Coussen F, Normand E, Marchal C, Costet P, Choquet D, Lambert M, Mege RM, Mulle C (2002) Recruitment of the kainate receptor subunit glutamate receptor 6 by cadherin/catenin complexes. *J Neurosci* **22:** 6426–6436

Coussen F, Perrais D, Jaskolski F, Sachidhanandam S, Normand E, Bockaert J, Marin P, Mulle C (2005) Co-assembly of two GluR6 kainate receptor splice variants within a functional protein complex. *Neuron* **47:** 555–566

Derkach VA, Oh MC, Guire ES, Soderling TR (2007) Regulatory mechanisms of AMPA receptors in synaptic plasticity. *Nat Rev Neurosci* **8:** 101–113

Fernandes HB, Catches JS, Petralia RS, Copits BA, Xu J, Russell TA, Swanson GT, Contractor A (2009) High-affinity kainate receptor subunits are necessary for ionotropic but not metabotropic signaling. *Neuron* **63:** 818–829

Gallyas Jr. F, Ball SM, Molnar E (2003) Assembly and cell surface expression of KA-2 subunit-containing kainate receptors. *J Neurochem* **86:** 1414–1427

Garcia EP, Mehta S, Blair LA, Wells DG, Shang J, Fukushima T, Fallon JR, Garner CC, Marshall J (1998) SAP90 binds and clusters kainate receptors causing incomplete desensitization. *Neuron* **21:** 727–739

Ghetti A, Heinemann SF (2000) NMDA-Dependent modulation of hippocampal kainate receptors by calcineurin and Ca(2+)/calmodulin-dependent protein kinase. *J Neurosci* **20:** 2766–2773

Hansel C, de Jeu M, Belmeguenai A, Houtman SH, Buitendijk GH, Andreev D, De Zeeuw CI, Elgersma Y (2006) alphaCaMKII is essential for cerebellar LTD and motor learning. *Neuron* **51:** 835–843

Hirbec H, Francis JC, Lauri SE, Braithwaite SP, Coussen F, Mulle C, Dev KK, Coutinho V, Meyer G, Isaac JT, Collingridge GL, Henley JM (2003) Rapid and differential regulation of AMPA and kainate receptors at hippocampal mossy fibre synapses by PICK1 and GRIP. *Neuron* **37:** 625–638

Jaskolski F, Coussen F, Nagarajan N, Normand E, Rosenmund C, Mulle C (2004) Subunit composition and alternative splicing regulate membrane delivery of kainate receptors. *J Neurosci* **24:** 2506–2515

Jaskolski F, Mayo-Martin B, Jane D, Henley JM (2009) Dynamin-dependent membrane drift recruits AMPA receptors to dendritic spines. *J Biol Chem* **284:** 12491–12503

Jaskolski F, Mulle C, Manzoni OJ (2005) An automated method to quantify and visualize colocalized fluorescent signals. *J Neurosci Methods* **146:** 42–49

Kornreich BG, Niu L, Roberson MS, Oswald RE (2007) Identification of C-terminal domain residues involved in protein kinase A-mediated potentiation of kainate receptor subtype 6. *Neuroscience* **146:** 1158–1168

Kristensen AS, Jenkins MA, Banke TG, Schousboe A, Makino Y, Johnson RC, Huganir R, Traynelis SF (2011) Mechanism of Ca(2+)/calmodulin-dependent kinase II regulation of AMPA receptor gating. *Nat Neurosci* **14:** 727–735

Kwon HB, Castillo PE (2008) Long-term potentiation selectively expressed by NMDA receptors at hippocampal mossy fiber synapses. *Neuron* **57:** 108–120

Lee HK, Takamiya K, He K, Song L, Huganir RL (2010) Specific roles of AMPA receptor subunit GluR1 (GluA1) phosphorylation sites in regulating synaptic plasticity in the CA1 region of hippocampus. *J Neurophysiol* **103:** 479–489

Lisman J, Schulman H, Cline H (2002) The molecular basis of CaMKII function in synaptic and behavioural memory. *Nat Rev Neurosci* **3:** 175–190

Luscher C, Xia H, Beattie EC, Carroll RC, von Zastrow M, Malenka RC, Nicoll RA (1999) Role of AMPA receptor cycling in synaptic transmission and plasticity. *Neuron* **24:** 649–658

Makino H, Malinow R (2009) AMPA receptor incorporation into synapses during LTP: the role of lateral movement and exocytosis. *Neuron* **64:** 381–390

Mammen AL, Huganir RL, O'Brien RJ (1997) Redistribution and stabilization of cell surface glutamate receptors during synapse formation. *J Neurosci* **17:** 7351–7358

Marchal C, Mulle C (2004) Postnatal maturation of mossy fibre excitatory transmission in mouse CA3 pyramidal cells: a potential role for kainate receptors. *J Physiol* **561**(Part 1): 27–37

Martin S, Henley JM (2004) Activity-dependent endocytic sorting of kainate receptors to recycling or degradation pathways. *EMBO J* **23:** 4749–4759

Martin S, Nishimune A, Mellor JR, Henley JM (2007) SUMOylation regulates kainate-receptor-mediated synaptic transmission. *Nature* **447:** 321–325

Melyan Z, Lancaster B, Wheal HV (2004) Metabotropic regulation of intrinsic excitability by synaptic activation of kainate receptors. *J Neurosci* **24:** 4530–4534

Mulle C, Sailer A, Perez-Otano I, Dickinson-Anson H, Castillo PE, Bureau I, Maron C, Gage FH, Mann JR, Bettler B, Heinemann SF (1998) Altered synaptic physiology and reduced susceptibility to kainate-induced seizures in GluR6-deficient mice. *Nature* **392:** 601–605

Nasu-Nishimura Y, Hurtado D, Braud S, Tang TT, Isaac JT, Roche KW (2006) Identification of an endoplasmic reticulum-retention motif in an intracellular loop of the kainate receptor subunit KA2. *J Neurosci* **26:** 7014–7021

Nasu-Nishimura Y, Jaffe H, Isaac JT, Roche KW (2010) Differential regulation of kainate receptor trafficking by phosphorylation of distinct sites on GluR6. *J Biol Chem* **285:** 2847–2856

Newton AJ, Kirchhausen T, Murthy VN (2006) Inhibition of dynamin completely blocks compensatory synaptic vesicle endocytosis. *Proc Natl Acad Sci USA* **103:** 17955–17960

Nicoll RA, Schmitz D (2005) Synaptic plasticity at hippocampal mossy fibre synapses. *Nat Rev Neurosci* **6:** 863–876

O'Brien JA, Lummis SC (2006) Biolistic transfection of neuronal cultures using a hand-held gene gun. *Nat Protoc* **1:** 977–981

Opazo P, Choquet D (2011) A three-step model for the synaptic recruitment of AMPA receptors. *Mol Cell Neurosci* **46:** 1–8

Opazo P, Labrecque S, Tigaret CM, Frouin A, Wiseman PW, De Koninck P, Choquet D (2010) CaMKII triggers the diffusional trapping of surface AMPARs through phosphorylation of stargazin. *Neuron* **67:** 239–252

Park Y, Jo J, Isaac JT, Cho K (2006) Long-term depression of kainate receptor-mediated synaptic transmission. *Neuron* **49:** 95–106

Perrais D, Veran J, Mulle C (2010) Gating and permeation of kainate receptors: differences unveiled. *Trends Pharmacol Sci* **31:** 516–522

Pinheiro PS, Lanore F, Veran J, Artinian J, Blanchet C, Crepel V, Perrais D, Mulle C (2012) Selective block of postsynaptic kainate receptors reveals their function at hippocampal mossy fiber synapses. *Cereb Cortex* (advance online publication 17 February 2012; doi:10.1093/cercor/bhs022)

Rebola N, Carta M, Lanore F, Blanchet C, Mulle C (2011) NMDA receptor-dependent metaplasticity at hippocampal mossy fiber synapses. *Nat Neurosci* **14:** 691–693

Rebola N, Lujan R, Cunha RA, Mulle C (2008) Adenosine A2A receptors are essential for long-term potentiation of NMDA-EPSCs at hippocampal mossy fiber synapses. *Neuron* **57:** 121–134

Rebola N, Sachidhanandam S, Perrais D, Cunha RA, Mulle C (2007) Short-term plasticity of kainate receptor-mediated EPSCs induced by NMDA receptors at hippocampal mossy fiber synapses. *J Neurosci* **27:** 3987–3993

Ren Z, Riley NJ, Garcia EP, Sanders JM, Swanson GT, Marshall J (2003) Multiple trafficking signals regulate kainate receptor KA2 subunit surface expression. *J Neurosci* **23:** 6608–6616

Rivera R, Rozas JL, Lerma J (2007) PKC-dependent autoregulation of membrane kainate receptors. *EMBO J* **26:** 4359–4367

Ruiz A, Sachidhanandam S, Utvik JK, Coussen F, Mulle C (2005) Distinct subunits in heteromeric kainate receptors mediate ionotropic and metabotropic function at hippocampal mossy fiber synapses. *J Neurosci* **25:** 11710–11718

Rumbaugh G, Vicini S (1999) Distinct synaptic and extrasynaptic NMDA receptors in developing cerebellar granule neurons. *J Neurosci* **19:** 10603–10610

Sachidhanandam S, Blanchet C, Jeantet Y, Cho YH, Mulle C (2009) Kainate receptors act as conditional amplifiers of spike transmission at hippocampal mossy fiber synapses. *J Neurosci* **29:** 5000–5008

Selak S, Paternain AV, Aller MI, Pico E, Rivera R, Lerma J (2009) A role for SNAP25 in internalization of kainate receptors and synaptic plasticity. *Neuron* **63:** 357–371

Shen K, Meyer T (1999) Dynamic control of CaMKII translocation and localization in hippocampal neurons by NMDA receptor stimulation. *Science* **284:** 162–166

Stoppini L, Buchs PA, Muller D (1991) A simple method for organotypic cultures of nervous tissue. *J Neurosci Methods* **37:** 173–182

Yamagata Y, Kobayashi S, Umeda T, Inoue A, Sakagami H, Fukaya M, Watanabe M, Hatanaka N, Totsuka M, Yagi T, Obata K, Imoto K, Yanagawa Y, Manabe T, Okabe S (2009) Kinase-dead knock-in mouse reveals an essential role of kinase activity of Ca2 + / calmodulin-dependent protein kinase IIalpha in dendritic spine enlargement, long-term potentiation, and learning. *J Neurosci* **29:** 7607–7618

Yan JZ, Xu Z, Ren SQ, Hu B, Yao W, Wang SH, Liu SY, Lu W (2011) Protein kinase C promotes N-methyl-D-aspartate (NMDA) receptor trafficking by indirectly triggering calcium/calmodulin-dependent protein kinase II (CaMKII) autophosphorylation. *J Biol Chem* **286:** 25187–25200

